International Journal of Pharmacology

ISSN 1811-7775

science alert

ansinet
Asian Network for Scientific Information

International Journal of Pharmacology 11 (8): 920-928, 2015
ISSN 1811-7775

RESEARCH ARTICLE OPEN ACCESS

DOI: 10.3923/ijp.2015.920.928

3D-QSAR Studies, Molecular Dynamics Simulation and Free Energy Calculation of APN Inhibitors

Qinglian Qu, Xianshuai Tang, Binhai Kuang, Shaohua Li and Guogang Tu
Department of Medicinal Chemistry, School of Pharmaceutical Science, Nanchang University, 461, BaYi Road, NanChang, 330006, People's Republic of China

ARTICLE INFO
Article History:
Received: July 21, 2015
Accepted: October 15, 2015

Corresponding Author:
Guogang Tu
Department of Medicinal Chemistry, School of Pharmaceutical Science, Nanchang University, 461, BaYi Road, NanChang, 330006, People's Republic of China

ABSTRACT
The MIFs was applied to a data set of 40 N-phenylhomophthalimide derivatives of APN inhibitors to generate the 3D-QSAR model at various 3D grid spacing. The cross-validated correlation coefficient q^2_{LMO} (0.6204) and r^2_{pred} (0.9810) were obtained at a 1.0 Å 3D grid spacing, indicating the statistical significance of this class of compounds. The calculated inhibitive activities showed a high degree of agreement with experimented values. Then, the 6 nsec MD simulation of protein-ligand complex and binding free energy analysis were carried out. The stable binding mode of the most active compound 21 was determined.

Key words: MIFs, APN inhibitor, 3D-QSAR, free energy, LMO

INTRODUCTION

APN, a zinc-containing proteolytic ectoenzyme, is called neutral aminopeptidase, based on the pH at which its maximal activity is observed. The most favorable substrates of APN are peptides having an alanine residue at the amino-terminal end (Lalu *et al*., 1986). The APN, also been named gluzincins, has the typical zinc-binding active site with the consensus amino acid sequence of Hisl-Glu2-Xaa3-Xaa4-His5-18 residues-Glu24, which is similar to that of metalloproteinases such as thermolysin. The His1 (the first His of the consensus amino acid sequence of the zinc-binding active site), His5 and Glu24 are the Zn^{2+} coordinating residues, while Glu2 is involved in catalysis. The functions of the enzyme depend on its location. In the synaptic membranes, the enzyme inactivates neuropeptides (enkephalins and endorphins) (Hooper, 1994). In intestinal brush border, APN degrades small peptides from the N-terminal end (Riemann *et al*., 1999). Recently, APN has been shown to be the major receptor for the enteropathogenic coronavirus TGEV (Delmas *et al*., 1992) and for human coronavirus 229E (Yeager *et al*., 1992) and has also been shown to be involved in invasion and metastasis of a variety of tumor cells (Menrad *et al*., 1993). The APN is expressed in malignant melanoma cells, but is absent from normal melanocytes. The enzyme is also expressed in macrophages and fibroblasts that exhibit high mobility in solid tissues (Matrisian, 1990). In fact, APN inhibitors have been reported to inhibit significantly the invasion of murine and human metastatic tumor cells into reconstituted basement membranes (Talmadge *et al*., 1986; Fujii *et al*., 1996). These findings suggest that neutral APN plays a crucial role in matrix degradation and invasion by tumor cells and that APN inhibitors may be useful for preventing the spread of malignant cells (Carl-McGrath *et al*., 2004; Hashida *et al*., 2002; Ishii *et al*., 2001).

The Quantitative Structure Activity Relationships (QSAR) are now modern media for drug design. The QSAR are the most important applications of chemometrics giving useful information for the design of new compounds acting on a specific target. The QSAR attempts to find a consistent relationship between biological activity and molecular properties (He and Jurs, 2005). Three-dimensional Quantitative Structure Activity Relationships (3D-QSAR) analysis is now the most widely used and improved technique (Kubinyi, 1993). Thus, QSAR models can be used to predict the activity of new compounds. Molecular docking and Molecular Dynamics (MD) simulation are used to study how a ligand is interacting with its biological target and to support the conclusions of QSAR studies (Kirkpatrick, 2004). The strength of a biomolecular interaction such as involved in

recognition or catalysis can be quantified in terms of its binding free energy and a range of computational approaches can be used to estimate binding free energies. The MM-PBSA approach has grown to be one of the most widely used methods to compute interaction energies and is often employed to study biomolecular complexes (Homeyer and Gohlke, 2012).

In this study, 3D-QSAR models for N-phenylhomophthalimide derivatives of APN inhibitors is introduced. In addition, the binding mode of the most activity compound 21 in APN binding site, obtained through docking, MD simulation experiments and binding free energies calculation, is discussed.

MATERIALS AND METHODS

Experimental data: All the compounds (Fig. 1) and associated activity data used in this study were obtained from literature (Shimazawa *et al*., 1999). The inhibitory activity data was reported as IC_{50}. The IC_{50} was converted to pIC_{50} by taking $\log(1/IC_{50})$, the pIC_{50} values were used as dependent variable in 3D-QSAR study. Especially many experimented pIC_{50} values in our dataset were set to 3.2 because the IC_{50} values had been assessed to be greater than 100 μg mL^{-1}. According to research methodology, 3D-QSAR model was carried out through Molecular Interaction Fields (MIFs) analysis by dividing the dataset of 40 molecules into training set of 33 molecules (82.5%) and test set of 7 molecules (17.5%) in a random manner. The structure and inhibitory activity of these compounds were given in Table 1 (the testing set is marked by *).

Alignment: The molecules were superimposed using the phar-based alignment b y the open3DALIGN tools (Tosco *et al*., 2011). The compound 21 was selected as the template to construct other compounds because of its high biological activity and representative chemical structure and the alignment was completed by open3DALIGN workstation. Except for some special notes, default values were chosen.

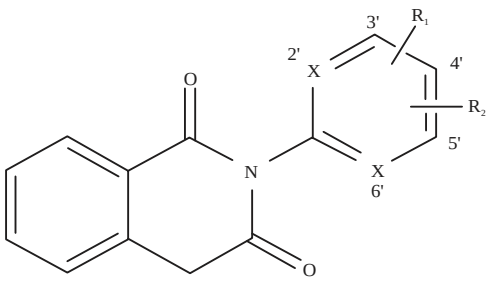

Fig. 1: N-phenylhomophthalimide derivatives of APN inhibitors

Generating MIFs: The MIFs are the interaction energies between a probe atom (or a molecule) and a set of aligned molecules, which are used to establish the 3D-QSAR equations. To generate the MIFs, a probe atom is systematically moved from one point to another for each aligned molecule within a defined 3D grid (Liton *et al*., 2013). At each grid point, the interaction energy is calculated between the probe and the target molecule. In this study, the 40 aligned molecules were placed in various 3D cubic lattice spacing. The steric (van der waals) and electrostatic (coulombic) interaction energies were calculated for each molecule at each grid point using an alkyl carbon probe (default) with automatically assigned charges using OpenBabel utilities. Energies lower than -40.0 kcal mol^{-1} and greater than 40.0 kcal mol^{-1} were cutoff, because a few high values in the dataset may severely bias the model.

The MIFs analysis described here was performed on open3DQSAR tools (Tosco and Balle, 2011) using Partial Least Square (PLS) (Stahle and Wold, 1987) technique through the NIPALS algorithm methodology (Wold *et al*., 2001). To obtain the 3D-QSAR models, PLS analysis was performed using steric and electrostatic field alone and also combination. The models were further improved by using Smart Region Definition (SRD) and Iterative Variable Elimination PLS (IVE-PLS) methods. Cross-validation in PLS was carried out using the Leave Many Mut method (LMO) (Clark, 2003) to check the predictive ability of the models and to determine the optimal number of components to be used in the final 3D-QSAR models. We carried out 20 LMO-cross-validation runs leaving at each run 1 of 5 randomly-composed groups of compounds out of the model (i.e., 20%) and predicted their activities via the reduced model. LMO-cross-validation is much more robust than LOO-cross-validation (Golbraikh and Tropsha, 2002). The quality of a model is expressed as the cross-validated correlation coefficient q^2. The optimal number of components is the largest value of q^2.

Molecular docking and MD simulations: Elucidation of ligand binding mechanisms is the necessary step to obtain more selective and potent drugs. So we made a molecular docking and molecular dynamics study of the most activity compound 21 with APN (PDBid: 4FYR) and further identified the critical amino acid residues for ligand binding. Docking was performed with AutoDock4.2 software package, which combines a rapid energy evaluation through precalculated grids of af nity potentials with a variety of search algorithms to nd suitable binding positions for a ligand on a given protein (Morris *et al*., 1998). When docking, APN was kept rigid, but all the torsional bonds in compound 21 were set free to perform exible docking. Polar hydrogens were added by using the hydrogens module in AutoDock Tools (ADT) for APN; after that, kollman united atom partial charges were assigned (La Motta *et al*., 2007). Docking of compound 21 to APN was

Table 1: Structure and APN inhibitory activity of N-phenylhomophthalimide derivatives

Compounds	X	R_1	R_2	pIC_{50} (Exp)	pIC_{50} (Cal)	Residues
1	CH CH	H	H	3.4030	3.3408	-0.0622
2	CH CH	2'-Me	H	3.7816	3.7678	-0.0138
3	CH CH	2'-Et	H	4.1728	4.2295	0.0567
4	CH CH	3'-Et	H	4.3551	4.3284	-0.0267
5	CH CH	4'-Et	H	3.2000	3.1961	-0.0039
6	CH CH	2'-iPr	H	3.7108	3.6140	-0.0968
7	CH CH	4'-iPr	H	3.2000	3.1176	-0.0824
8	CH CH	2'-OMe	H	4.6341	4.6869	0.0528
9	CH CH	3'-OMe	H	4.4488	4.4842	0.0354
10	CH CH	4'-OMe	H	4.5344	4.5293	-0.0051
11	CH CH	2'-SMe	H	5.4975	5.3790	-0.1185
12*	CH CH	3'-SMe	H	4.5487	4.7028	0.1541
13	CH CH	4'-SMe	H	4.6594	4.6484	-0.011
14*	CH CH	3'-CH_2OH	H	3.9641	3.9296	-0.0345
15	CH CH	2'-Me	6'-Me	4.4837	4.5774	0.0937
16*	CH CH	2'-Me	5'-Me	4.3588	4.7051	0.3463
17	CH CH	2'-Me	4'-Me	4.2031	4.2080	0.0049
18	CH CH	2'-Me	3'-Me	3.9461	4.1069	0.1608
19*	CH CH	3'-Me	4'-Me	4.0653	4.3983	0.333
20	CH CH	3'-Me	5'-Me	5.2472	5.3465	0.0993
21	CH CH	2'-Et	6'-Et	6.3877	6.3369	-0.0508
22*	CH CH	2'-Et	5'-Et	4.8334	5.1737	0.3403
23	CH CH	2'-Et	4'-Et	4.1768	4.2045	0.0277
24	CH CH	2'-iPr	6'-iPr	4.9624	4.9792	0.0168
25	CH CH	2'-Me	6'-Et	5.8121	5.9008	0.0887
26*	CH CH	2'-Me	6'-iPr	5.5748	5.2872	-0.2876
27	CH CH	2'-tBu	5'-tBu	3.2000	3.1860	-0.014
28	CH CH	3'-tBu	5'-tBu	4.6795	4.6648	-0.0147
29	CH CH	2'-OMe	5'-OMe	4.9676	5.0973	0.1297
30	CH CH	2'-OMe	4'-OMe	4.7826	4.5577	-0.2249
31	CH CH	3'-OMe	4'-OMe	3.2000	3.3374	0.1374
32	CH CH	3'-OMe	5'-OMe	4.7485	4.5015	-0.247
33	CH CH	3',4',5'-tri-OMe		3.2000	3.3613	0.1613
34	CH CH	2'-Cl	6'-Cl	3.8413	3.8662	0.0249
35	CH CH	2'-F	6'-F	3.2000	3.2804	0.0804
36	CH CH	2',3'-fused-Ph		5.2274	5.1358	-0.0916
37*	N N	3'-OMe	5'-OMe	3.2000	2.7669	-0.4331
38	CH N	3'-Me	5'-Me	4.8686	4.9159	0.0473
39	N N	3'-Me	5'-Me	3.2000	3.0773	-0.1227
40	N N	3'-Me	5'-OMe	4.3987	4.3672	-0.0315

Exp: Experimental, Cal: Calculated, *Testing set

carried out using the empirical free energy function and the lamarckian genetic algorithm with a standard protocol. Fifty independent docking runs were carried out. Results were clustered according to the 1.0 Å Root Mean Square Deviation (RMSD) criterion. All torsion angles for compound 21were considered exible. The grid maps representing the proteins in the actual docking process were calculated with AutoGrid. The grids (one for each atom type in the ligand plus one for electrostatic interactions) were chosen to be suf ciently large to include not only the active site but also signi cant portions of the surrounding surface. The dimensions of the grids were thus 60×60×60 Å, with a spacing of 0.375 Å between the grid points.

Based on the docking results, MD simulation was carried out with the gromacs 4.6.5 (Van Der Spoel *et al*., 2005) suite of programs using the amber99SB force field (Hornak *et al*., 2006). The APN-21 complex was placed in the center of octahedron box and solvated by TIP3P water model (Jorgensen *et al*., 1983). The Na^+ counterions were added to satisfy the electroneutrality condition. Using the leapfrog algorithm in the NPT ensemble, each component, compound 21, APN, H_2O and Na^+, was separately coupled. The v-rescale temperature coupling and parrinello-rahman pressure coupling (the coupling constants were both set to 0.1) were used to keep the system in a stable environment (300 K, 1 bar). Distance restraints were to applied to maintain the Zn-ion in the correct ligation state. The nominal charge of +2 was used for Zn-ion. The Zn-chelating histidine residues were protonated at the δ-nitrogen (Manzetti *et al*., 2003). The APN-21 complex was rst energy minimized with the steepest descent method; then a 100 psec position restraining simulation was carried out restraining the APN by a 1000 kJ mol^{-1} $Å^2$ harmonic constraint to relieve close contacts before the actual simulation; nally, a 6 nsec MD simulation was performed. During these steps, the Particle Mesh Ewald (PME) method for long-range electrostatics, a 14 Å cutoff for van der waals

interactions, a 9Å cutoff for coulomb interaction and the LINCS algorithm for bond constraints were used (Hess *et al*., 1997). Periodic boundary conditions were applied to avoid edge effects.

Binding free energy calculations: For APN-21 complex system, free energy calculations were performed for 200 snapshots extracted from the last 2 nsec stable MD trajectory using g_mmpbsa (Kumari *et al*., 2014). The van der waals radius of the catalytic Zn-ion was set to 1.77 (Batsanov, 2001). For each snapshot, the free energy was calculated for each molecular species (complex, protein and ligand) and the binding free energy is computed by Eq. 1. ΔG_{MM}, the molecular mechanics energy, was calculated by the electrostatic and van der waals interactions. ΔG_{sol}, the solvation free energy, was composed of the polar and the nonpolar contributions. Polar solvation free energy could be obtained by solving the poisson-boltzmann equation for MM/PBSA method, whereas nonpolar solvation free energy was determined using Solvent Accessible Surface Area (SASA) model. TΔS represented the entropy term:

$$\Delta G_{bind} = \Delta G_{MM} + \Delta G_{sol} - T\Delta S \quad (1)$$

RESULT AND DISCUSSION

3D-QSAR study: To develop an effective 3D-QSAR model, some parameters such as the cross-validated correlation coefficient (q^2), non-cross-validated correlation coefficient (r^2), Standard Deviation of the Error of Predictions (SDEP) and Standard Deviation on SDEP (SD on SDEP) have been taken under consideration. The LMO-cross-validation was carried out for 3D-QSAR model. Then the number of components identified in the LMO-cross-validation process was used in the final non-cross-validated PLS run. The optimal number of components was determined by selecting the highest q^2 value. The statistical results of MIFs studies were summarized in Table 2. The correlation between the calculated activities and the experimented activities was depicted in Fig. 2 and Table 1.

The MIFs-based PLS calculation resulted in several models and among them, the final model selection is an important issue. To obtain the 3D-QSAR models, PLS analysis was performed using each of the steric and electrostatic MIFs alone and also in combination varying on 3D grid spacing. Six types of model were produced on varying the grid spacing. All the models comparatively showed good statistical results except the model 2 and model 3 (Table 2). The external predictive ability of the MIFs model is extremely important in terms of the applicability of the MIFs model. Therefore, it was decided to use the r^2_{pred} as a criterion for final selection of the best model. As reflected by the Table 3, all the models showed comparatively good r^2_{pred} values except model 3. Therefore

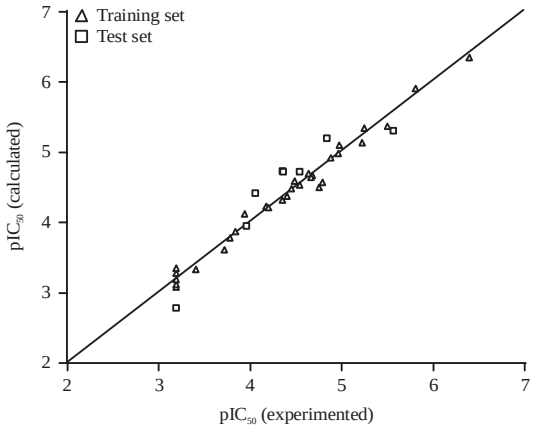

Fig. 2: Graph of experimented versus calculated pIC_{50} value

model 1, which uses both steric and electrostatic fields on 1.0Å grid spacing, was chosen as the working MIFs model, whose validity and predictability were assessed by the r^2 value of 0.9465 and q^2_{LMO} value of 0.6204 with 8 components and a SD on SDEP of 0.0434. The steric and electrostatic contributions were 37.7 and 63.3%, respectively, meanwhile model 1 has the highest r^2_{pred} value of 0.9810 and hence the lowest SDEP value of 0.0953 for the test set.

A graphical inspection of the experimented with calculated pIC_{50} values indicated that the overall fit of the molecule was satisfactory for model 1 (Fig. 2). The results of the analyses showed that the best model is model 1; that is to say, the combined fields (steric and electrostatic) at a 1.0 Å gave the best statistical results. Therefore, model 1 was selected as the best MIFs model. Compared with the QSAR results of literature, our 3D-QSAR modeling have good predictive ability (Zhu *et al*., 2008; Xu *et al*., 2012).

The 3D-QSAR contour maps were generated to visualize the field distribution of the generated model and provide information to direct the development of novel selective APN inhibitors. Figure 3a presents the steric contour map around superposed compounds. In the PLS analysis, steric unfavorable regions are depicted in yellow, whereas favorable regions are in green. Nonsubstituted N-phenylhomophthalimide (compound 1) was almost inactive. The steric effect of substituents at the 2'- and 6'-positions is extremely important for potent activity. The 2', 6'-diethylphenyl derivative (compound 21) showed the most potent APN-inhibitory activity. The effect of the two ethyl groups introduced at the 2'- and 6'-positions seems to be specific, because the corresponding regioisomers (2', 5'-isomer: 22 and 2', 4'-isomer: 23), as well as the 2', 6'-dimethyl (compound 15) and 2',6'-diisopropyl (compound 24) analogs all have much weaker APN-inhibitory activity than compound 21. The potency of APN-inhibitory activity decreased in the order of 2'-ethyl (compound 3) >> 2'-methyl

Table 2: Statistical analysis of training set through MIFs studies

Model No.	3D-Grid spacing	Compounds	Components	q^2_{LMO}	r^2	SD on SDEP	Contribution	
							Steric	Electrostatic
1	1.0	40	8	0.6204	0.9465	0.0434	36.7%	63.3%
2	1.0	40	8	0.4207	0.9721	0.0540	100.0	0.0
3	1.0	40	8	0.1621	0.9042	0.0545	0.0	100.0
4	1.5	40	8	0.6207	0.9902	0.0365	36.4%	63.6%
5	2.0	40	8	0.6211	0.9786	0.0472	36.3%	63.7%
6	2.5	40	8	0.6293	0.9820	0.0355	35.3%	64.7%

SD: Standard deviation, SDEP: Standard deviation of the error of predictions

Table 3: Statistical analysis of test set through MIFs studies

Model No	3D-Grid spacing	r^2_{pred}	SDEP	Contribution	
				Steric	Electrostatic
1	1.0	0.9810	0.0953	36.7%	63.3%
2	1.0	0.8952	0.2237	100.0	0.0
3	1.0	0.3158	0.5716	0.0	100.0
4	1.5	0.9408	0.1681	36.4%	63.6%
5	2.0	0.8986	0.2201	36.3%	63.7%
6	2.5	0.8412	0.2753	35.3%	64.7%

SEP: Standard deviation of the error of predictions

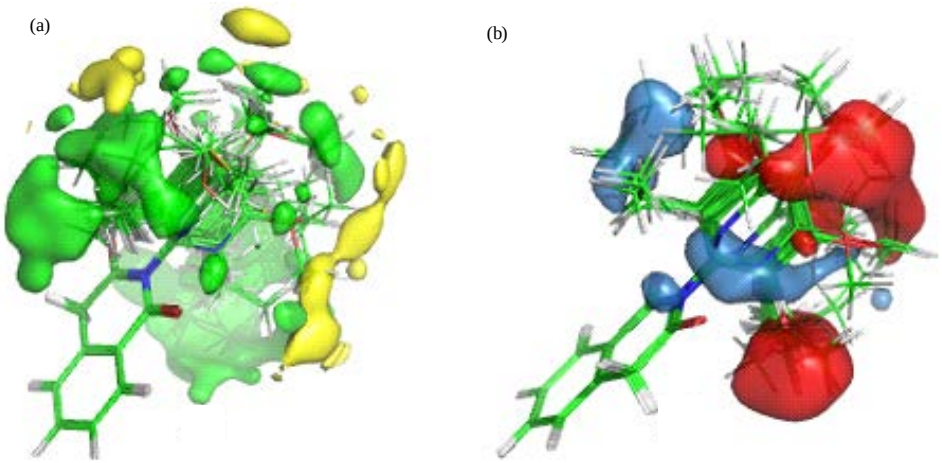

Fig. 3(a-b): Illustration of the PLS pseudocoefficient contour maps of the 3D-QSAR model with the superposed compounds from both training and test sets (level: ±0.0002)

(compound 2) >2'-isopropyl (compound 6) analogs for monosubstituted N-phenylhomophthalimides. The corresponding 4'-alkylated regioisomers (compound 6 and 7) did not show APN-inhibitory activity.

The PLS electrostatic contour map (Fig. 3b) includes main red region and blue regions. A great attention should be paid to the big red region which indicates that the presence of negatively charged group would increase the bioactivity remarkably. For monosubstituted N-phenylhomophthalimides, introduction of electron-withdrawing group increased the activity. For example, the activity increased in the order of 2'-methylthio (compound 11), 3'-methylthio (compound 12), 4'-methylthio (compound 13) >2'-methoxyl (compound 8), 3'-methoxyl (compound 9), 4'-methoxyl (compound 10) >2'-ethyl (compound 3), 3'-ethyl (compound 4), 4'-ethyl (compound 5) respectively. Compound 29, 30 show higher activity than compound 16, 17, mainly for introduction of electron-withdrawing dimethoxyl at 2',5'-position and 2',4'-position respectively. In addition, introduction of electron-withdrawing F, Cl did not increase the bioactivity remarkably. This observation is consistent with the experimental activity in literature (Shimazawa *et al*., 1999). Compared with the MD simulation results, the 3D-QSAR modeling was performed to give further validation of the binding mode and provide a structural framework for understanding the structure-activity relationship of the inhibitors.

Molecular docking and MD simulation: It is difficult to explain the molecular mechanism of inhibitor binding to APN on the basis of the docking data alone, because the protein

molecule remains rigid during the docking. To investigate the binding features of the inhibitors, we performed 6 nsec MD simulation of the APN-21 complexes which was the result of molecular docking.

The Root Mean Square Deviation (RMSD) of the atomic positions with respect to the starting structure was calculated. The obtained RMSD values for backbone atoms of the APN are about 2.0 Å and relatively stable after 2 nsec, indicating that the molecular systems were well behaved thereafter. The RMSD values of compound 21 atoms are about 0.5 Å and then leveled off after that. This indicates that, after an initial increase in the magnitude of APN and ligand atoms fluctuation, the system reached an equilibrium state characterized by the RMSD profile (Fig. 4).

There are two hydrophobic domains beside the catalytic activity center of APN, called pockets S_1 and S_1', respectively (Mou *et al*., 2010). The compound 21 could interact with the active binding site which is consistent with highly potent drug Bestatin (Bauvois and Dauzonne, 2006). The binding mode of compound 21 with APN is shown in Fig. 5. It can be seen that compound 21 is anchored into the active binding site via a network of hydrogen bonds and hydrophobic

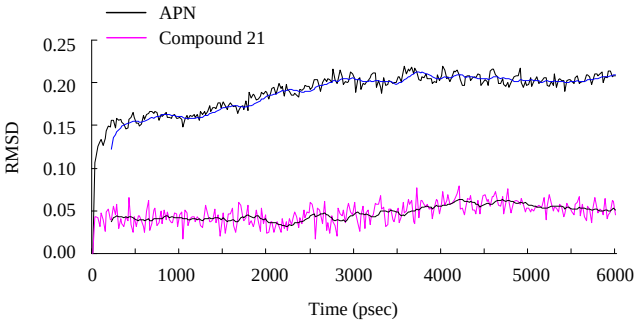

Fig. 4: RMSD of APN backbone atoms and heavy atoms in compound 21

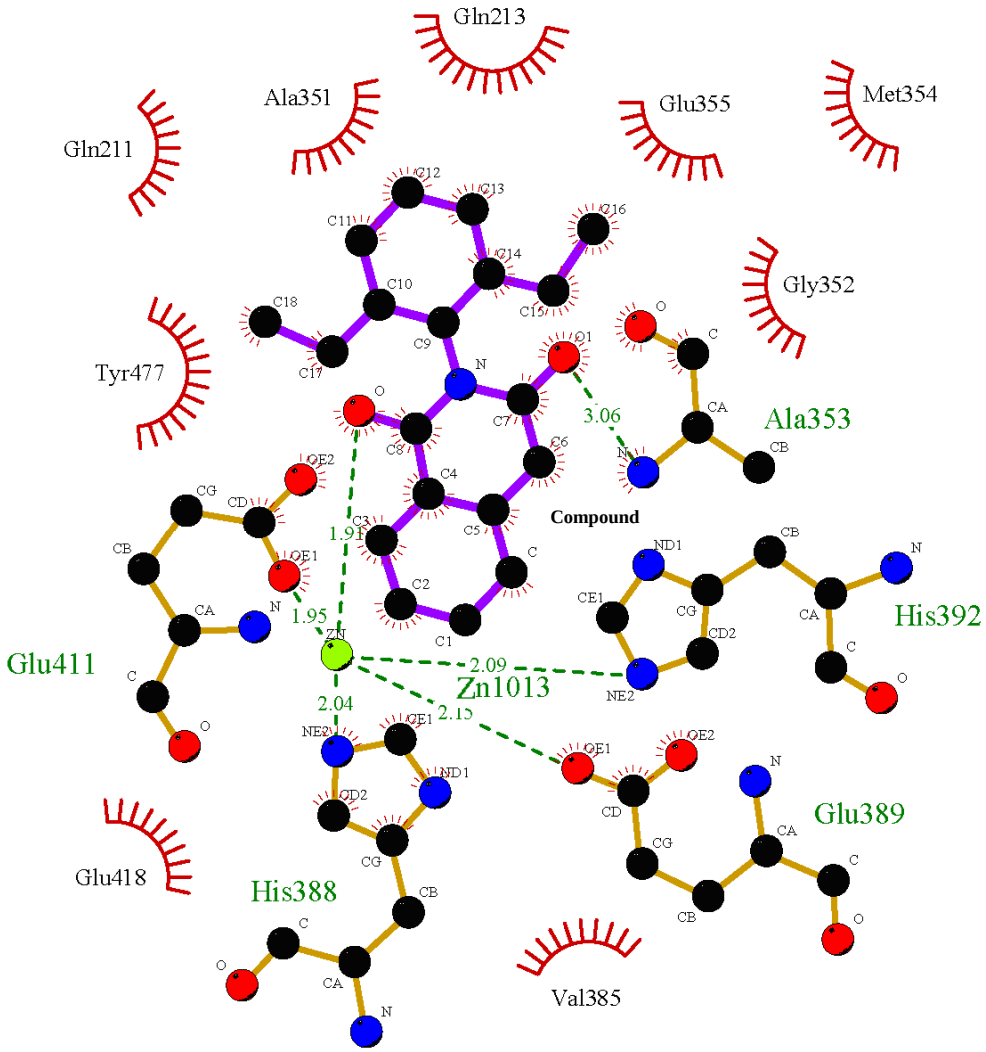

Fig. 5: Diagram of the hydrogen bonds and hydrophobic interactions of the compound 21 with active-site residues in APN

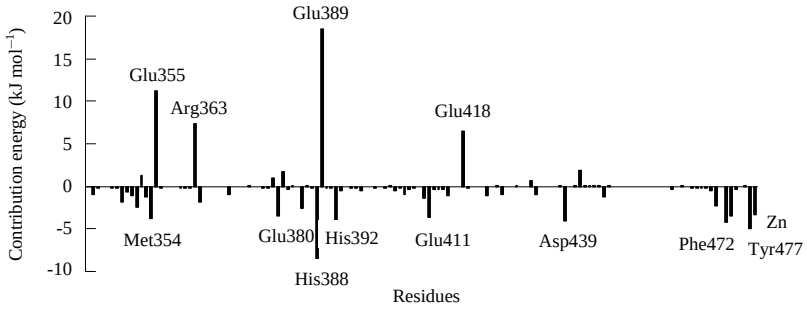

Fig. 6: Energy of each residue contribution to the binding of compounds 21 with APN active site

interactions. The carbonyl oxygen of compound 21 coordinates with the catalytic Zn-ion with the distance of 1.91 and another carbonyl oxygen forms a hydrogen bond with polar H atom of Ala353. At the same time, hydrophobic interactions were formed. In addition the catalytic Zn-ion coordinates with His388, His392, Glu389 and Glu411, which is the same with the crystal structure of 4FYR.

Interaction mechanism based on the binding free energy analysis: The predicted binding free energy is -149.95 kJ mol^{-1}, composed of van der waal energy -165.76 kJ mol^{-1}, electrostatic energy -130.58 kJ mol^{-1}; polar solvation energy 160.07 kJ mol^{-1} and SASA energy -13.68 kJ mol^{-1}. The individual energy term nonpolar interactions, including van der Waals energy and nonpolar solvation energy, is of vital importance to the binding process. On the contrary, the sum of the electrostatic interactions, which consists of the electrostatic energy and the polar solvation energy, is unfavorable to the binding. The favorable coulomb interactions are counteracted by the unfavorable electrostatics of desolvation. It is found that the sum of the electrostatic interactions is 29.49 kJ mol^{-1}, whereas nonpolar interactions is -179.54 kJ mol^{-1}. So the intermolecular van der waals contribution is most significant. The observation is consistent with the large hydrophobic binding surface between compound 21 and APN as well as Bestatin and APN (Ito *et al*., 2006; Chen *et al*., 2012). In order to gain further insight into ligand-protein interaction, binding free energy was decomposed to ligand-residue pairs (Fig. 6). The energy decomposition analysis shows that the main contributions are -3.73, -3.43, -8.57, -4.43, -3.58, -4.07, -4.25 and -5.02 kJ mol^{-1} from residues Met354, Glu380, His388, His392, Glu411, Asp439, Phe472 and Tyr477, respectively. Especially the contribution of the catalytic Zn-ion is -3.30 kJ mol^{-1}. It is shown that Glu355, Arg363, Glu389 and Glu418 are in disfavor with the binding for compound 21. Compared with the 3D-QSAR, MD simulation and binding free energy analysis better explained the binding mechanism with the residues and chemical group interactions of the inhibitors.

CONCLUSION

In this study, carried out MIFs studies for 40 N-phenylhomophthalimide derivatives against experimented biological activities. The phar-based alignment with varying the 3D grid spacing method was used to provide the model for MIFs analysis. Our present studies have established that the model derived through MIFs studies is quite reliable and significant. We have investigated that the PLS analysis at 1.0Å 3D grid spacing by Open3DQSAR tools has presented an quite statistical results in terms of q^2_{LMO} and r^2_{pred} values and showed a high degree of agreement with the experimented inhibitory activities. In addition, the molecular interaction mechanism of inhibitor binding to APN active binding site was explained on the basis of MD simulation and binding free energy analysis. Our results suggested that inhibitor can exactly bind to the active binding site of APN to display inhibitory activity and the van der waals interactions could be driving force for the binding of inhibitor with APN.

ACKNOWLEDGMENT

The project was supported by National Natural Science Foundation of China (81160383, 81260469), Jiangxi Province Science Foundation (20132BAB205076) and the science and technology research project of Jiangxi Provincial Educational Department (GJJ14161).

REFERENCES

Batsanov, S.S., 2001. Van der Waals radii of elements. Inorg. Mater., 37: 871-885.

Bauvois, B. and D. Dauzonne, 2006. Aminopeptidase-N/CD13 (EC 3.4.11.2) inhibitors: Chemistry, biological evaluations and therapeutic prospects. Med. Res. Rev., 26: 88-130.

Carl-McGrath, S., U. Lendeckel, M. Ebert, A.B. Wolter, A. Roessner and C. Rocken, 2004. The ectopeptidases CD10, CD13, CD26 and CD143 are upregulated in gastric cancer. Int. J. Oncol., 25: 1223-1232.

Chen, L., Y.L. Lin, G. Peng and F. Li, 2012. Structural basis for multifunctional roles of mammalian aminopeptidase N. Proc. Natl. Acad. Sci. USA., 109: 17966-17971.

Clark, R.D., 2003. Boosted leave-many-out cross-validation: The effect of training and test set diversity on PLS statistics. J. Comput.-Aided Mol. Des., 17: 265-275.

Delmas, B., J. Gelfi, R. L'Haridon, L.K. Vogel, H. Sjostrom, O. Noren and H. Laude, 1992. Aminopeptidase N is a major receptor for the enteropathogenic coronavirus TGEV. Nature, 357: 417-420.

Fujii, H., M. Nakajima, T. Aoyagi and T. Tsuruo, 1996. Inhibition of tumor cell invasion and matrix degradation by aminopeptidase inhibitors. Biol. Pharmaceut. Bull., 19: 6-10.

Golbraikh, A. and A. Tropsha, 2002. Beware of q^2! J. Mol. Graph. Modell., 20: 269-276.

Hashida, H., A. Takabayashi, M. Kanai, M. Adachi and K. Kondo *et al*., 2002. Aminopeptidase N is involved in cell motility and angiogenesis: Its clinical significance in human colon cancer. Gastroenterology, 122: 376-386.

He, L. and P.C. Jurs, 2005. Assessing the reliability of a QSAR model's predictions. J. Mol. Graphics Modell., 23: 503-523.

Hess, B., H. Bekker, H.J. Berendsen and J.G.E.M. Fraaije, 1997. LINCS: A linear constraint solver for molecular simulations. J. Comput. Chem., 18: 1463-1472.

Homeyer, N. and H. Gohlke, 2012. Free energy calculations by the molecular mechanics Poisson-Boltzmann surface area method. Mol. Inform., 31: 114-122.

Hooper, N.M., 1994. Families of zinc metalloproteases. FEBS Lett., 354: 1-6.

Hornak, V., R. Abel, A. Okur, B. Strockbine, A. Roitberg and C. Simmerling, 2006. Comparison of multiple Amber force fields and development of improved protein backbone parameters. Proteins: Struct. Funct. Bioinform., 65: 712-725.

Ishii, K., S. Usui, Y. Sugimura, H. Yamamoto, K. Yoshikawa and K. Hirano, 2001. Inhibition of Aminopeptidase N (AP-N) and urokinase-type Plasminogen Activator (uPA) by zinc suppresses the invasion activity in human urological cancer cells. Biol. Pharmaceut. Bull., 24: 226-230.

Ito, K., Y. Nakajima, Y. Onohara, M. Takeo and K. Nakashima *et al*., 2006. Crystal structure of aminopeptidase N (proteobacteria alanyl aminopeptidase) from *Escherichia coli* and conformational change of methionine 260 involved in substrate recognition. J. Biol. Chem., 281: 33664-33676.

Jorgensen, W.L., J. Chandrasekhar, J.D. Madura, R.W. Impey and M.L. Klein, 1983. Comparison of simple potential functions for simulating liquid water. J. Chem. Phys., 79: 926-935.

Kirkpatrick, P., 2004. Gliding to success. Nat. Rev. Drug Discovery, 3: 299-299.

Kubinyi, H., 1993. 3D QSAR in Drug Design: Volume 1: Theory Methods and Applications. Springer Science and Business Media, New York, ISBN: 9789072199140, Pages: 759.

Kumari, R., R. Kumar and A. Lynn, 2014. *G_mmpbsa*-a GROMACS tool for high-throughput MM-PBSA calculations. J. Chem. Inform. Model., 54: 1951-1962.

La Motta, C., S. Sartini, L. Mugnaini, F. Simorini and S. Taliani *et al*., 2007. Pyrido[1,2-*a*]pyrimidin-4-one derivatives as a novel class of selective aldose reductase inhibitors exhibiting antioxidant activity. J. Med. Chem., 50: 4917-4927.

Lalu, K., S. Lampelo and T. Vanha-Perttula, 1986. Characterization of three aminopeptidases purified from maternal serum. Biochimica Biophysica Acta (BBA)-Protein Struct. Mol. Enzymol., 873: 190-197.

Liton, M.A.K., A.C. Bhowmick and M.A. Ali, 2013. 3D-QSAR MIFs studies on 3,5-substituted-1,4,2-dioxazoles derivatives using Open3DQSAR tools. Universal J. Chem., 1: 71-76.

Manzetti, S., D.R. McCulloch, A.C. Herington and D. van der Spoel, 2003. Modeling of enzyme-substrate complexes for the metalloproteases MMP-3, ADAM-9 and ADAM-10. J. Comput.-Aided Mol. Des., 17: 551-565.

Matrisian, L.M., 1990. Metalloproteinases and their inhibitors in matrix remodeling. Trends Genet., 6: 121-125.

Menrad, A., D. Speicher, J. Wacker and M. Herlyn, 1993. Biochemical and functional characterization of aminopeptidase N expressed by human melanoma cells. Cancer Res., 53: 1450-1455.

Morris, G.M., D.S. Goodsell, R.S. Halliday, R. Huey, W.E. Hart, R.K. Belew and A.J. Olson, 1998. Automated docking using a Lamarckian genetic algorithm and an empirical binding free energy function. J. Comput. Chem., 19: 1639-1662.

Mou, J., H. Fang, Y. Liu, L. Shang, Q. Wang, L. Zhang and W. Xu, 2010. Design, synthesis and primary activity assay of bi- or tri-peptide analogues with the scaffold L-arginine as amino-peptidase N/CD13 inhibitors. Bioorg. Med. Chem., 18: 887-895.

Riemann, D., A. Kehlen and J. Langner, 1999. CD13-not just a marker in leukemia typing. Immunol. Today, 20: 83-88.

Shimazawa, R., H. Takayama, Y. Fujimoto, M. Komoda and K. Dodo *et al*., 1999. Novel small molecule nonpeptide aminopeptidase N inhibitors with a cyclic imide skeleton. J. Enzyme Inhibition, 14: 259-275.

Stahle, L. and S. Wold, 1987. Partial least squares analysis with cross-validation for the two-class problem: A Monte Carlo study. J. Chemometrics, 1: 185-196.

Talmadge, J.E., B.F. Lenz, R. Pennington, C. Long, H. Phillips, M. Schneider and H. Tribble, 1986. Immunomodulatory and therapeutic properties of bestatin in mice. Cancer Res., 46: 4505-4510.

Tosco, P. and T. Balle, 2011. Open3DQSAR: A new open-source software aimed at high-throughput chemometric analysis of molecular interaction fields. J. Mol. Model., 17: 201-208.

Tosco, P., T. Balle and F. Shiri, 2011. Open3DALIGN: An open-source software aimed at unsupervised ligand alignment. J. Comput.-Aided Mol. Des., 25: 777-783.

Van Der Spoel, D., E. Lindahl, B. Hess, G. Groenhof, A.E. Mark and H.J.C. Berendsen, 2005. GROMACS: Fast, flexible and free. J. Comput. Chem., 26: 1701-1718.

Wold, S., M. Sjostrom and L. Erikson, 2001. PLS-regression: A basic tool of chemometrics. Chemometrics Intell. Lab. Syst., 58: 109-130.

Xu, Y., L. Zhang, M. Li, W. Xu, H. Fang and L. Shang, 2012. QSAR studies of aminopeptidase N/CD13 (APN) inhibitors with the scaffold 3-phenylpropane-1,2-diamine and molecular docking. Med. Chem. Res., 21: 1000-1015.

Yeager, C.L., R.A. Ashmun, R.K. Williams, C.B. Cardellichio, L.H. Shapiro, A.T. Look and K.V. Holmes, 1992. Human aminopeptidase N is a receptor for human coronavirus 229E. Nature, 357: 420-422.

Zhu, H.W., H. Fang, L. Wang, W.X. Hu and W.F. Xu, 2008. 3D-QSAR study with pharmacophore-based molecular alignment of hydroxamic acid-related phosphinates that are aminopeptidase N inhibitors. Drug Discoveries Therapeut., 2: 52-57.